Millimeter-wave phase-imaging interferometer for the GAMMA 10 tandem mirror

doi: 10.1063/1.1142172

Millimeter-wave phase-imaging interferometer for the GAMMA 10 tandem mirror

K. Hattori,[a] A. Mase, A. Itakura, M. Inutake, and S. Miyoshi
Plasma Research Center, University of Tsukuba, Tsukuba 305, Japan

K. Uehara, T. Yonekura, H. Nishimura, K. Miyashita, and K. Mizuno
Research Institute of Electrical Communication, Tohoku University, Sendai 980, Japan

(Received 23 April 1991; accepted for publication 10 September 1991)

A millimeter-wave phase-imaging interferometer has been developed for the study of density profiles of the GAMMA 10 tandem mirror. The interferometer uses a 70-GHz klystron oscillator and a quasi-optical transmission system. The probe beam is expanded so as to fill an orthogonal view of a plasma cross section. The view is imaged onto a detector array. The detector array consists of beam-lead GaAs Schottky barrier diodes bonded to antennas fabricated using photolithographic techniques on a fused-quartz substrate. Two types of antennas, bow-tie and Yagi–Uda antennas have been used in order to provide an effective matching to millimeter-wave beams, and compared for the performance of an imaging system. The interferometers have been applied to the central-cell and plug-cell plasmas of GAMMA 10.

I. INTRODUCTION

In recent years, phase-imaging interferometers have been used and constructed in several plasma experiments in order to measure multichord line-integrated electron densities. The first example was a CO_2 laser interferometer using a 15-element PbSnTe detector array which was applied to a high-density arc plasma.[1] A far-infrared laser interferometer with a 20-element integrated microbolometer array has been applied to a tokamak plasma by the UCLA group.[2] A set of cylindrical lenses or off-axis parabolic mirrors produces a sheet-like beam to illuminate the entire cross section of a plasma. The phase distribution produced by the plasma is imaged onto a detector array. The number of channels is determined by the number of detectors in the array and a single set of optics is used for all channels. This eases problems in conventional multichannel interferometers such as cost and spatial resolution.

We have developed a millimeter-wave phase-imaging interferometer using a Schottky barrier diode array for the first time and applied to a tandem mirror plasma. Millimeter-wave imaging techniques become important in remote sensing, atmospheric radiometry, radio astronomy, and radars as well as in plasma diagnostics.

The manuscript is organized as follows. In Sec. II, we describe the phase-imaging systems applied to the central-cell and plug-cell plasmas of GAMMA 10. The results of the tests on the imaging arrays using bow-tie and Yagi–Uda antennas and the system calibration using a dielectric object are presented in Sec. III. Section IV gives experimental results of line-density profiles. In Sec. V we summarize.

[a]Present address: Nobeyama Radio Observatory, National Astronomical Observatory, Nobeyama, Nagano 384-13, Japan.

II. DESCRIPTION OF THE PHASE-IMAGING SYSTEMS

A. Optical system

The principles for designing an optical system are as follows. A probe beam should cover the majority of plasma cross section. Cross section of the beam at the vacuum windows must be small enough compared with the size of the windows. Spherical aberration of the optical system must be as small as possible specifically on the detector array. The optical systems have been designed and estimated by using a ray-tracing code as well as a Gaussian-beam propagation theory.[3]

We have constructed two different phase-imaging systems for GAMMA 10 plasmas. Figure 1(a) shows a schematic view of the system designed for the central-cell plasma. A 400-mW microwave of frequency $f = 70$ GHz is launched through a transmitter horn, and divided by a polyethylene beamsplitter BS_1 into two beams, a probe beam and a reference beam. The probe beam is expanded in one dimension using polyethylene cylindrical lenses L_2 to L_5 so that it covers the majority of the plasma cross section, 360 mm in diameter, which is determined by the limiter installed in the central cell. The vacuum windows are made of fused-quartz with 400 mm$\times$140 mm. The distance between the vacuum windows is 1.2 m. The probe beam and the reference beam are superimposed coaxially by a beamsplitter BS_2. A similar set of lenses L_6 to L_9 and an objective lens L_{10} demagnify the beam again and cast the image onto a detector array. A substrate lens is used on the back side of the detector array in order to eliminate a crosstalk between neighboring antennas and spherical aberration or coma.[4]

The system applied to the plug-cell plasma is shown in Fig. 1(b). In this system, number of lenses and optical parameters are different from the central-cell system since the distance between the vacuum windows, 3.0 m, and the plasma radius, 200 mm, are different. The reference beam

 0034-6748/91/122857-05$02.00

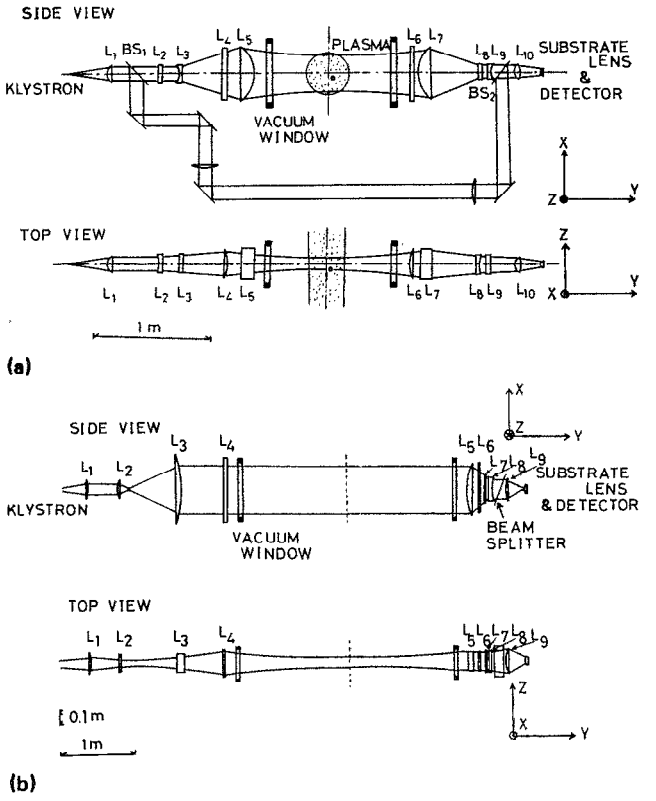

FIG. 1. Schematic view of the millimeter-wave phase-imaging systems at (a) the central cell and (b) the plug cell.

is obtained from a waveguide-type directional coupler and transported by using oversized waveguide.

B. Detector array antennas

Detector-array antennas of two types are used for the present phase-imaging interferometers. One is bow-tie antenna array[2,4] with 11 elements, and the other is Yagi–Uda antenna array[5] with 10 elements. The detector array consists of beam-lead GaAs Schottky barrier diodes bonded to each antenna which is monolithically fabricated on a fused-quartz substrate of 25 mm×25 mm. The spacing between the antennas 2.14 mm is determined from the Nyquist sampling theorem given by

$$T=\lambda f_{\#}/n, \tag{1}$$

where λ is the wavelength in free space, $f_{\#}$ is the effective f number of the objective lens, and n is the refractive index of the quartz substrate.

The layout of the bow-tie antenna array is shown in Fig. 2. The resistive antenna impedance of 150 Ω, which is obtained for a 60° bow angle on a fused-quartz ($\epsilon=4$) substrate, is adopted in order to provide the best matching to the diode detectors.

The layout of the Yagi–Uda antenna array is shown in Fig. 3. It consists of a radiator element on the one side of the substrate and a director on the other side, between the substrate and the substrate lens. The dimensions of the antenna elements shown in Fig. 3 are also determined in

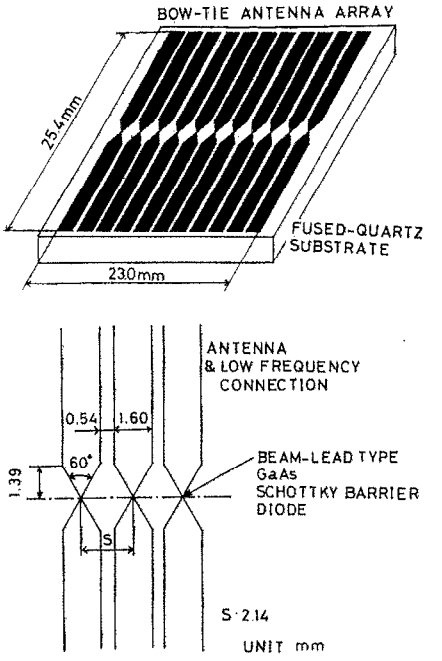

FIG. 2. Layout of the detector array using bow-tie antennas (top) and magnification view of the element (bottom).

order to provide impedance matching to the diodes and beam pattern matching to the optics.

III. TEST OF PHASE-IMAGING INTERFEROMETER

A. Optical system

The beamwidth of the power pattern is measured with a waveguide antenna at several positions along the beam

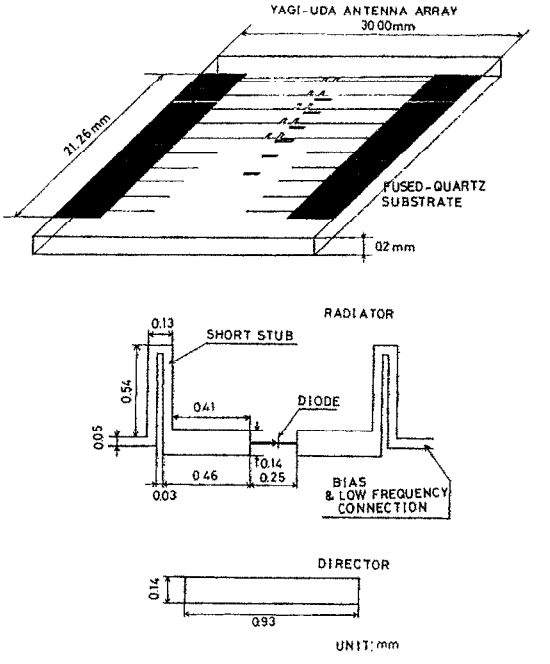

FIG. 3. Layout of the detector array using Yagi–Uda antennas (top) and magnification view of the element (bottom). It consists of a radiator element on the dielectric-air interface and a director on the other side.

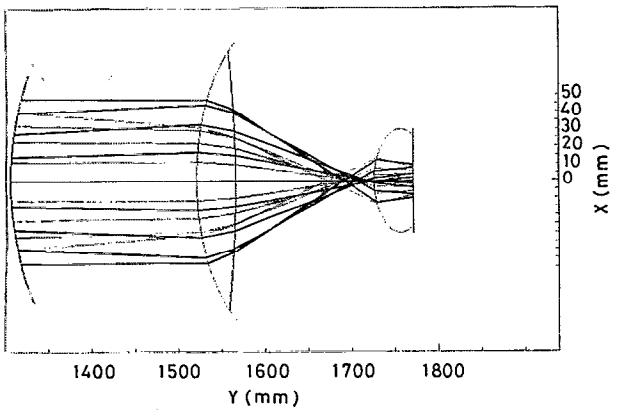

FIG. 4. Ray tracing using a geometric optics theory applied for the central-cell system.

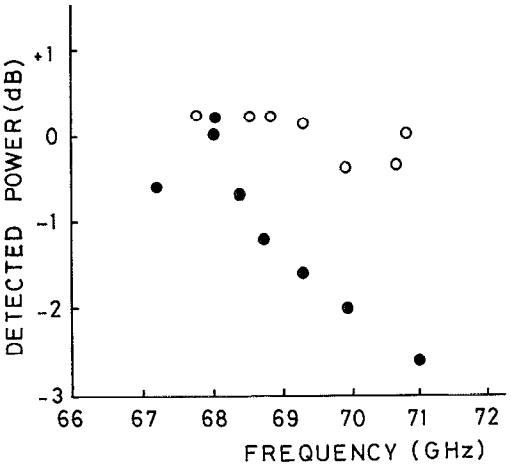

FIG. 5. Video responsivity of the detectors as a function of frequency. Circles represent the data obtained from the bow-tie antenna array, and dots represent the data obtained from the Yagi–Uda antenna array.

propagation. The values at the plasma center are 350 mm $\times$90 mm for the central-cell system and 320 mm$\times$120 mm for the plug-cell system, respectively. The beamwidth in the vertical direction covers most of the plasma radius.

The results of ray-tracing using a geometrical optics theory are shown in Fig. 4 for the central-cell system. Thick lines are the rays without refraction effect of a plasma, and thin lines are with it. The plasma is assumed to have a uniform and axisymmetric density of 3×10^{18} m^{-3}. An image has a one-to-one correspondence with an object, that is, a position across the plasma corresponds to a point on the image plane, and the displacement of the rays due to the diffraction is negligibly small at the five channels near the optical axis. The ray tracing at the plug cell is also estimated similarly. The optimization of the system is done so as to obtain a good final image at both cells.

Magnifications of the central-cell and plug-cell optical systems are designed to be 20 and 17.2, respectively. The values agree with the experimental values within 4% error, which are determined by the ratio of the movement of a point source across the object plane and that of an image across the image plane.

B. Characteristics of detector array antennas

The video responsivity of the detectors is shown in Fig. 5 as a function of frequency. It is confirmed that the detector using bow-tie antennas have wider responsivity than the one using Yagi–Uda antennas as expected. Similar responsivity is obtained at a frequency band of 40 GHz for the bow-tie antennas. The peak video responsivity of $\simeq$60 V/W is evaluated from the input power to the objective lens. This value should increase when the best matching between the incident beam and the antenna pattern is obtained. The characteristics of the heterodyne detection are not measured in the present experiment. It has been shown that the diode has 4.0-dB conversion loss at 20 GHz with 1–2 GHz IF and an LO power of 5 mW. The maximum cut-off frequency of the diode is estimated to be 2300 GHz.[6]

The spatial resolutions of the detectors are estimated from a measurement of the Airy pattern by using the plug-cell system. A Gunn oscillator is located at the position corresponding to the plasma center. The source is imaged onto each array antenna. The examples of the Airy pattern are plotted in Figs. 6(a) and 6(b). The theoretical curves correspond to the Airy function which gives an intensity distribution of a point image by an ideal lens having circular aperture of diameter d, that is,

$$h(x)=\left(\frac{2J_1(kdx/2z')}{kdx/2z'}\right)^2, \tag{2}$$

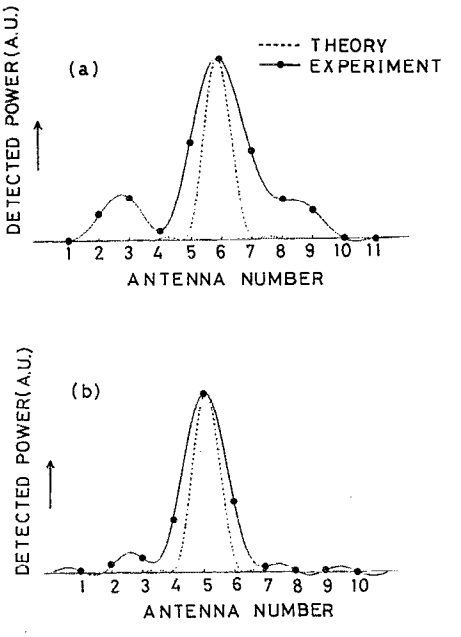

FIG. 6. Measurement of Airy pattern: (a) bow-tie antenna array, (b) Yagi–Uda antenna array. Dots represent the measured points. The solid lines represent the fitting curves drawn by using Eq. (3). The dotted lines are calculated from Eq. (2).

where J_1 is the Bessel function of the first order, k^{-1} is the wavelength at the image plane, and x and z' are the distance from the optical axis to the image plane and from the lens to the image plane, respectively. The fitting curve is drawn by using the Whittaker–Shannon sampling theorem given by[7]

$$E(x)=\sum_{n=-\infty}^{\infty} E\left(\frac{n}{2f_c}\right)\mathrm{sinc}\left[2f_c\left(x-\frac{n}{2f_c}\right)\right], \qquad (3)$$

where $E(n/2f_c)$ is the sampled data value, and $\mathrm{sinc}(x) = \sin \pi x/\pi x$. The discrepancy of the image between the experimental points and the theoretical curves may be due to the following reasons: (i) the image is disturbed by an error of the responsivity of each diode detectors, (ii)the image is detected by antennas with a finite size of the aperture, and (iii) the displacement of an optical axis. The side-lobe of the pattern is bigger for the bow-tie antenna than for the Yagi–Uda antenna probably due to the reason that the image obtained by the bow-tie antennas is disturbed by a crosstalk between neighboring antennas.

From the definition of Rayleigh limits,[8] the spatial resolution of the antenna array is estimated to be $r_a = 5.7$ mm for the bow-tie antenna and 4.6 mm for the Yagi–Uda antenna, respectively, where r_a indicates the distance which we can distinguish two point sources on the detector array. Spatial resolution of the detector using the Yagi–Uda antenna is better than that using the bow-tie antenna.

C. Imaging of a test object

We measure phase distribution of a Teflon bar of 103 mm in width and 1.0 mm in thickness, and the refractive index of $n=1.43$ in order to show the performance of the present phase-imaging system. Here, the plug-cell system with the Yagi–Uda antenna array is utilized for the measurement. Figure 7 shows the image of the bar target as it is moved across the object plane which corresponds to the plasma center. The bar target is moved 73.6 mm each time at the object plane. On the image plane, this shift corresponds to two channels on the array antenna.

Theoretical phase distribution is given by[2,9]

$$\phi(x)=(2/\pi)^{1/2}\phi_0\{\mathrm{Si}[2\pi f_c(x+a)]-\mathrm{Si}[2\pi f_c(x-a)]\}, \qquad (4)$$

where x is the location on the image plane, $2a$ is the width of the bar, $\mathrm{Si}(x)$ is the sine integral, and $\phi_0 = (2\pi)^{1/2}(n-1)t/\lambda_0$ is the pulse height. A good agreement is obtained between the theory and the experiment, and the image of the bar target moves corresponding to the movement of the target across the object plane.

IV. DENSITY PROFILES IN GAMMA 10 PLASMAS

The phase-imaging interferometers described above have been installed at the midplane of the central cell ($z=0$ m) and at the west-plug cell ($z=9.7$ m) in the GAMMA 10 tandem mirror, where the z axis coincides with the machine axis. A millimeter-wave interferometer with scanning horn antennas is used for the cross calibration at the central cell.

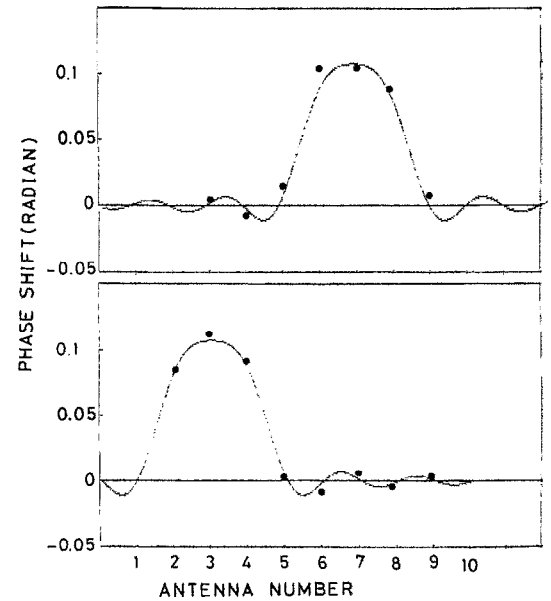

FIG. 7. Phase distribution of a Teflon bar with 104 mm in width and 1.0 mm in thickness. Dots represent the measured points. The dotted lines represent the theoretical curves calculated from Eq. (4). The location of the bar is 73.6 mm above the object plane (top) and 73.6 mm below the object plane (bottom).

Figure 8 shows the time evolutions of the line-density measured with the phase-imaging interferometer and the scanning interferometer at the central cell. The agreement between the two is satisfactory when it is taken into account that the two interferometers view different chords, that is, the horizontal and vertical chords. The time development of the line-density profile is shown in Fig. 9. A good agreement between the profile data from the two interferometers is obtained. The heating systems of GAMMA 10 are operated as follows: Initially, a plasma is injected by magnetoplasma dynamic guns (PG) from both

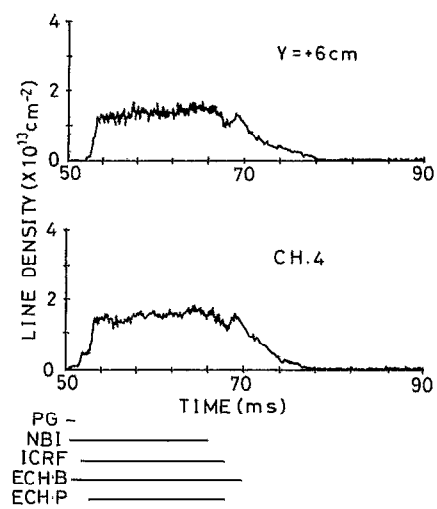

FIG. 8. Time evolution of the line-density measured with the scanning interferometer (top) and the phase-imaging interferometer (bottom).

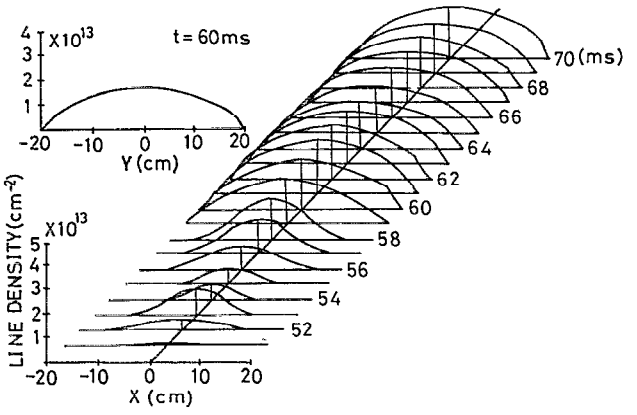

FIG. 9. Time evolution of the line-density profile at the central cell.

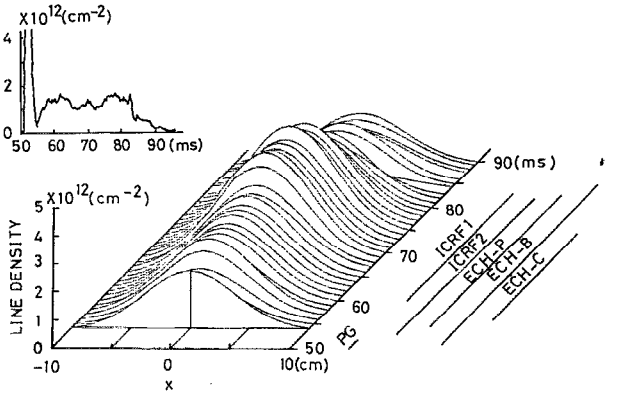

FIG. 10. Time evolution of (a) the line density and (b) the line-density profile at the plug cell.

ends of the machine. Neutral beams (NBI) produce sloshing ions in the plug/barrier cells. Four gyrotrons providing electron cyclotron resonance heating with a frequency of 28 GHz are used to generate magnetically trapped hot electrons that produce thermal barrier potential depression ($\omega = 2\omega_{ce}$, ECH-B) and warm electrons for positive potential peaks that confine central cell ions ($\omega = \omega_{ce}$, ECH-P in the plug/barrier cells. Ion cyclotron range of frequency (ICRF) is employed to heat ions in the central cell. The narrow profile of the gun-produced plasma expands to a half-maximum diameter of about 30 cm after additional heating.

Figure 10 shows the similar data obtained at the plug cell. In this case, the half-maximum diameter of the steady-state plasma is about 10 cm. The diameter corresponds to an incident beam-width of the ECH-P gyrotrons.

The spatial resolutions of the systems are estimated to be $\simeq$2.0 cm at the central cell and $\simeq$1.5 cm at the plug cell, respectively. These values are difficult to obtain by using conventional multichannel interferometers.

V. DISCUSSION

In summary, millimeter-wave phase-imaging interferometers have been constructed and applied to the GAMMA 10 tandem mirror. Two types of integrated detector arrays using bow-tie and Yagi–Uda antennas have been tested in order to demonstrate the ability of the phase-imaging system. The spatial resolution of Yagi–Uda antenna was found to be better than that of bow-tie antenna. The time evolution and radial profiles of the line density have been successfully measured at the central cell and plug cell of GAMMA 10.

ACKNOWLEDGMENTS

The authors deeply acknowledge the members of the GAMMA 10 group of University of Tsukuba for their collaboration. Special thanks are due to Professor T. Ishihara of University of Tsukuba for his discussion and encouragement. They would also like to thank Dr. Y. Harada and his group of SANYO Electric Co., Ltd., Semiconductor Research Center for supplying the detectors.

[1] C. A. J. Hugenholtz and B. J. H. Meddens, Rev. Sci. Instrum. **53**, 171 (1982).
[2] P. E. Young, D. P. Neikirk, P. P. Tong, D. B. Rutledge, and N. C. Luhmann, Jr., Rev. Sci. Instrum. **56**, 81 (1985).
[3] H. Kogelnik and T. Li, Appl. Opt. **10**, 1550 (1966).
[4] D. B. Rutledge and M. S. Muha, IEEE Trans. Antennas Propag. **AP-30**, 535 (1982).
[5] K. Uehara, T. Yonekura, H. Nishimura, K. Miyashita, and K. Mizuno, in *Proceedings of the 3rd Asia-Pacific Microwave Conference* (Tokyo, Japan, 1990), p. 365.
[6] Y. Harada, Ph. D. thesis, Tohoku University, 1989 (in Japanese).
[7] J. W. Goodman, *Introduction to Fourier Optics* (McGraw–Hill, New York, 1968).
[8] M. Born and E. Wolf, *Principles of Optics*, 6th ed. (Pergamon, Oxford, 1980).
[9] P. E. Yong, Ph.D. thesis, University of California at Los Angeles, 1984.